VNU Journal of Science: Earth and Environmental Sciences
Journal homepage: https://js.vnu.edu.vn/EES

Original Article

Analysis of Geomorphic Factors Related to Seismic Activity in Lai Chau Hydropower Reservoir in the Period 2015 - 2024

Bui Van Duan[1], Dinh Quoc Van[1], Grzegorz Lizurek[2], Izabela Nowaczyńska[2], Jan Wiszniowski[2], Vi Van Vung[1], Le Ba Manh[1], Nguyen Thuy Linh[1], Vu Minh Tuan[1], Nguyen Thanh Hai[1], Nguyen Anh Duong[1,*]

[1]*Institute of Earth Sciences, Vietnamese Academy of Science and Technology (IES VAST), 84 Chua Lang, Dong Da, Hanoi, Vietnam*
[2]*Institute of Geophysics, Polish Academy of Sciences (IG PAS), Kssiecia Janusza 64, 01-452 Warszawa, Poland*

Received 21st January 2025
Revised 17th March 2025; Accepted 29th April 2025

Abstract: Following the reservoir impoundment, the seismic activity in the Lai Chau reservoir area and its vicinity has increased significantly. The changes in frequency of local earthquakes depends on: i) The type of rocks below the reservoir; ii) The slip tendency of faults in the reservoir area; iii) The Coulomb stress change on faults in the reservoir area; and iv) The history of the reservoir filling and spillage. The results show that the granite massif of the Phu Si Lung complex is located below the upstream area of the reservoir at a depth of about 3,000-4,000 m; when water percolates down through this type of rocks, it will cause some fractures in the rock to become saturated with water, making stress in the rock reach the failure threshold. Under the impact of the modern regional tectonic stress field, the faults connected to the reservoir (F-1, F-2, F-3, F-4) tend to slip at moderate to high rates, and the Coulomb stress change is also clearly shown on these faults. These factors, together with the annual fluctuations in the reservoir water level between the rainy and dry seasons, have mutual influences, triggering the earthquakes to occur in the Lai Chau reservoir area and its vicinity in the period 6/2015 - 6/2024.

Keywords: Earthquake, tectonic, fault, reservoir, stress field.

1. Introduction

Lai Chau reservoir began built in 2011. This is the lower terrace of Pac Ma Hydropower and the upper terrace of Son La Hydropower. The reservoir is located on the main stream of the Da river in Nam Nhun and Muong Te districts, Lai

* Corresponding author.
E-mail address: duongnaigp@gmail.com

https://doi.org/10.25073/2588-1094/vnuees.5282

Chau province (Figure 1). The dam of the reservoir is 137m high. The total capacity of the reservoir is 1.215 billion m^3. The reservoir began water impoundment on June 20, 2015 and reached the full supply level elevation of 295m above mean sea level on October 19, 2015.

The study area is located at the northern edge of the Indosinian geoblock which is separated from the South China geoblock by the Red River deep fault zone. During the Cenozoic, the tectonic movement of the Indosinian geoblock was directly controlled by the collision between the Indian and Eurasian continents. Tapponnier et al., [1-3] established a Cenozoic tectonic model for the East Asian region (see Figure 2). This model is considered as a consequence of the collision between the Indian and Eurasian continents. The nature of the collision shows not only the simple translational movement of the hard plates, but also the horizontal displacement, compression, rotation, and complex deformation of lithospheric blocks propagating along large fault zones, forming a complex and differentiated Neotectonic structural plan. Therefore, it can be concluded that Lai Chau reservoir is located in an active tectonic area.

The reservoir impoundment often affects the stability of geological structures (faults, dikes, etc.) inside and around the reservoir, which can lead to triggered earthquakes, but this is not an inevitable consequence of damming [4]. Until 2017, only 232 reservoir-triggered earthquakes were reported worldwide, in which 9 events had $M \geq 6.0$; 27 events had $5.0 \leq M \leq 5.9$; 56 events had $4.0 \leq M \leq 4.9$; and 129 events had $M < 4.0$ [5-7]. In Vietnam, reservoir-triggered earthquakes with magnitude $4.0 \leq M \leq 4.9$ have also been recorded at Hoa Binh and Tranh River 2 hydropower reservoirs [8-11].

Figure 1. Location of Lai Chau reservoir.

After the Lai Chau reservoir impoundment, seismic activity has increased in the reservoir area and its vicinity. Earthquakes occurred frequently in June 2020 in the upstream of the reservoir (Muong Te and Nam Khao communes), about 52 km northwest of the dam site. There have been a number of studies on seismic activity in this area, for example, Lizurek et al., (2019) and Telesca et al., (2023) focused on calculating and comparing the b-value before and after the reservoir filling to examine the relationship between reservoir filling and earthquakes [12, 13]. Therefore, studying the factors related to seismic activity in

the Lai Chau reservoir area in recent times is necessary. This study will focus on analyzing and assessing the factors related to the occurrence of earthquakes in the specific conditions of the Lai Chau reservoir area, namely: i) The type of rocks below the reservoir; ii) The slip tendency of faults in the reservoir area; iii) The Coulomb stress change on faults in the reservoir area; and iv) The history of the reservoir filling and spillage. The main purpose is to clarify the relationship between reservoir filling and seismic activity at the Lai Chau reservoir in recent times.

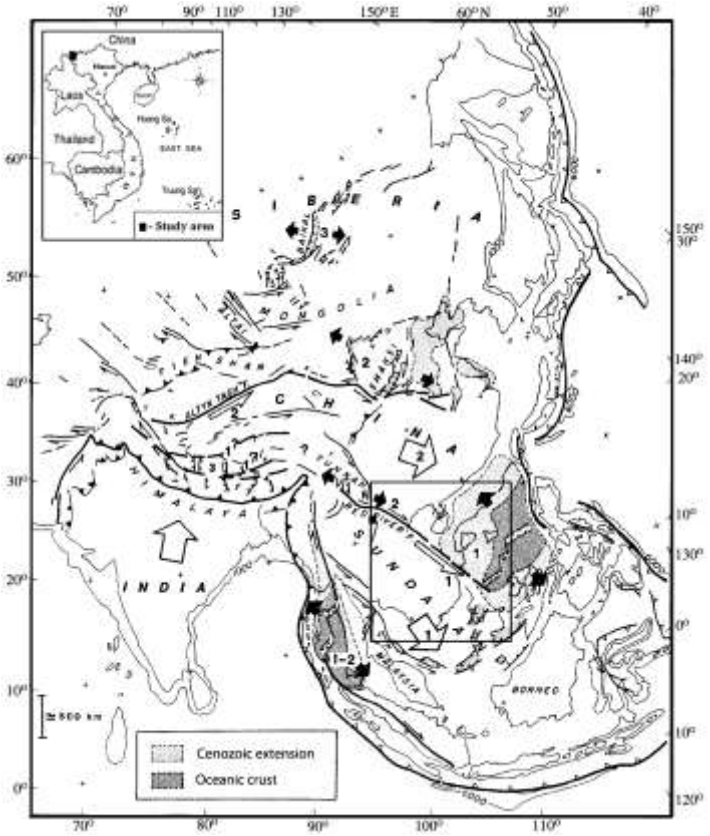

Figure 2. Study area on the tectonic plan and Cenozoic major faults in East Asia (modified from Tapponnier et al., 1982).

2. Data and Methodology

2.1. Data

Lai Chau reservoir lies entirely on the Muong Te tectonic block. The eastern part of the block is bounded by the Lai Chau - Dien Bien sub-longitudinal fault. The northern part of the block extends towards the Chinese territory. The western and southwestern parts of the block extend towards the Lao PDR territory. In Vietnam, from the northeast to the southwest, the Muong Te block is divided into three tectonic structural zones: Phu Si Lung zone, Muong Mo zone and Muong Nhe zone [14]. Lai Chau reservoir lies on the border area between the Phu Si Lung zone and the Muong Mo zone that are separated by the Thuong Song Da fault zone. This is a large-scale fault zone - the second order [15]. The fault extends from Chinese territory to Vietnam. It runs along the Da river valley through Muong Te, Kan Ho, then begins to branch in the fan shape near Muong Mo, and is finally bounded by the Lai Chau - Dien Bien

fault. The fault zone is clearly shown on the tectonic structural plan and on the modern topography.

In this zone, geological formations are fractured by the fault, forming large-scale shear zone and crumple zone, which are superimposed by the brittle deformation of tectonic cataclasis or tectonic brecciation in some places [15]. This fault zone is considered to be a seismogenic zone in the Northwest Vietnam [14, 16]. In this paper, the Thuong Song Da fault zone is divided into major fault segments (F-1, F-2, F-3) and minor fault segments (F-4, F-5, F-6, F-7), see Figure 3. These fault segments are established on the basis of DEM analysis and previous research results, including: Results of fault survey (supplementary) serving the design and construction of the Lai Chau Hydropower Plant [15]; and Results of assessing active fault systems in the area, establishing a map of seismogenic faults in Muong Te district [17]. Some basic characteristics of F-1, F-2, F-3, F-4, F-5, F-6 and F-7 faults are summarized and presented in Table 1 below.

Table 1. The geometry of the main faults in Lai Chau reservoir area

No.	Fault	Strike (°)	Length (km)	Depth (km)	Dip angle (°)/ Dip direction	Slip mechanism (N_2-Q)
1	F-1	132	25.4	15 - 30	80/NE	Dextral strike-slip – Reverse
2	F-2	114	47.3	15 - 30	80/ENE	Dextral strike-slip – Reverse
3	F-3	138	29.4	15 - 30	75/NE	Dextral strike-slip – Reverse
4	F-4	172	27.9	8 - 12	70/WSW	Normal
5	F-5	124	19.9	8 - 12	75/SW	Normal – Dextral strike-slip
6	F-6	155	19.6	8 - 12	75/ENE	Normal
7	F-7	172	25.6	8 - 12	75/WSW	Normal

Lai Chau reservoir is located in the Northwest Vietnam - the region with active seismic activity. This is confirmed in many different studies such as: [18, 19, 14]. Earthquake data in the Lai Chau reservoir area and its vicinity, before the reservoir filing to an elevation of 295 m (from 1900 to May 2015), were collected from the Final Report of the state-level independent project on earthquake and ground motion forecasting in Vietnam, as well as the Supplementary Report on determining design earthquake parameters for the Lai Chau Hydropower Plant Project during the technical design stage [19, 16]; Website of the International Seismological Center (ISC Bulletin: event catalogue search) [20]. Earthquake data after the reservoir filling (from June 2015 to March 2024) are collected from the following sources: i) Earthquake catalog of the ad hoc research project: Assessing the cause of the earthquake in Muong Te on June 16, 2020 and proposing solutions to minimize related risks, coded 01/2021/DX headed by Dr. Pham The Truyen [21]; and ii) Results of additional processing of earthquake data in the implementation of the VAST International Cooperation Task on Science, coded QTPL01.01/22-23 headed by Dr. Nguyen Anh Duong. The results show that 88 events with magnitude M = 2.0 - 4.9 were recorded in the Lai Chau reservoir area and its vicinity from 1961 to March 2024, in which 16 events occurred before 2015 (see Appendix). The spatial distribution of these earthquakes is presented in Figure 3. With the collected earthquake data, it can be seen that before the reservoir filling (1961 - 2014), 14 events with magnitude M_S = 2.8 - 4.7 and 2 events with M_L = 2.0 - 2.1 were recorded in the reservoir area; after the reservoir filling, there were 72 events with M_L = 2.0 - 4.9. This shows that the seismic activity in the Lai Chau reservoir area and its vicinity before the reservoir filling was at a medium - low level. After the reservoir filling, the seismic activity has increased. It indicates that the earthquake occurrence is related to the reservoir impoundment.

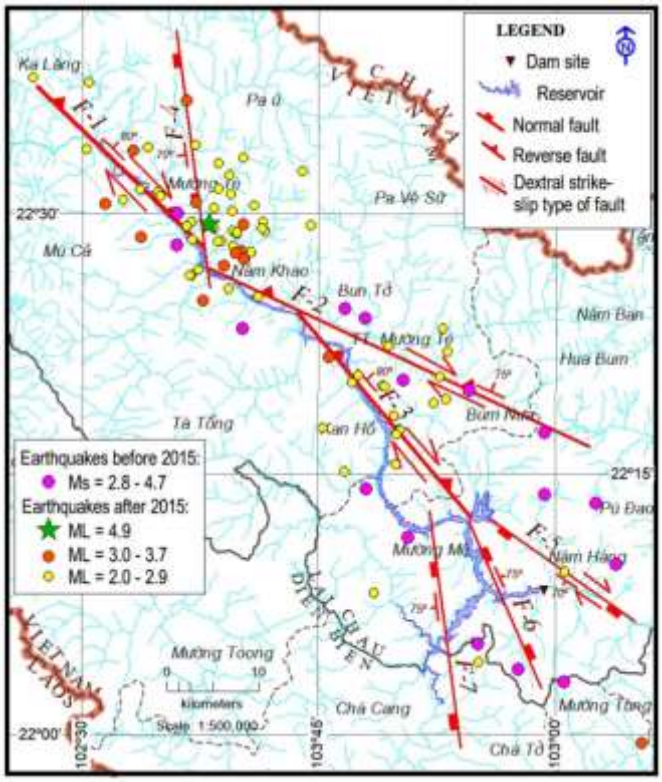

Figure 3. Map of faults and earthquake epicenters in Lai Chau reservoir area.

2.2. Methodology

Besides traditional methods such as geological map analysis, tectonic data analysis, earthquake data analysis, we also use the following methods:

2.2.1. Method of Coulomb Stress Change Calculation

The Coulomb stress change on the fault was built into the COULOMB program by Toda et al., (2011) based on the elastic half-space theory proposed by Okada (1992) and the Coulomb stress failure criterion proposed by King et al. (1994) [22-24]. Failure on the fault occurs when there is a large change in Coulomb stress which is determined by the formula:

$$\Delta CFS = \Delta\tau_s + \mu'\Delta\sigma_n \quad (1)$$

where ΔCFS is the Coulomb stress change on the faults, $\Delta\tau_s$ is the shear stress change, $\Delta\sigma_n$ is the normal stress change, and μ' is the apparent friction coefficient on the faults, μ' = μ(1-B), B is the Skempton's coefficient varying from B = 0 (dry surface layer) to B = 1 (water-saturated surface layer), μ is the friction coefficient. Since previous studies have shown that changes in μ' have little impact on the spatial distribution of Coulomb stress [22, 25], in this paper we take μ' = μ.

According to the Coulomb criterion, a fault tends to become active when the Coulomb stress on the fault surface reaches a critical value. A stress increase of 50kPa is sufficient to cause an earthquake [24]. The calculations are performed in an elastic, isotropic and homogeneous half-space. The method is developed to calculate displacement, strain and static stress at any depth caused by fault slip, magma intrusion, dike extension or contraction.

2.2.2. Method of Analyzing Slip Tendency on Fault Surface in 3D Space

Most earthquakes in the reservoirs are caused by the reactivation of pre-existing faults

rather than the formation of new ones [26]. The method was developed by Neves et al., (2009) as a subroutine of the COULOMB program based on the definition of slip tendency on fault surface by Morris et al. (1996) [26, 27]. The slip tendency on fault surface is defined as the ratio of the shear stress (τ) to the normal stress (σ_n) on the fault surface and is denoted by T_s,

$$T_S = \frac{\tau}{\sigma_n} \quad (2)$$

Accordingly, when $T_s \geq 0.5$, the fault tends to slip. Details of the method and algorithm can be found in [27].

3. Results

3.1. Type of Rocks Below The Reservoir

Table 2. Earthquake occurrence probability of rocks below the reservoirs [4]

Type of rocks	Earthquake occurrence probability (%)
Crystalline rock	39.13
Volcanic rock	12.17
Limestone	39.13
Terrigenous sedimentary rock	9.565

According to Qiu (2012) global statistical results from 115 triggered earthquakes occurring in reservoir areas, among the four types of rocks located below the reservoirs (crystalline rock, limestone, volcanic rock and terrigenous sedimentary rock), crystalline rock and limestone are the two types of rocks that are most likely to experience earthquakes (both accounting for 39.13%) [4], see Table 2.

Limestone is the most vulnerable rock to chemical dissolution by water. When the rock is chemically dissolved, its cohesion is reduced, i.e., friction is reduced, leading to a weakening of the strength on the fault [28]. The dissolved material can also be washed away by flowing water, causing the rock fractures to widen, reducing the strength of the rock, promoting the slip to occur earlier and eventually the occurrence of earthquakes. Most crystalline rocks, especially granites, are not considered to be porous. In a large granite body, more than 80% of the water flow is already contained in a few major fractures [29]. Even a small addition of water can cause these fractures to become saturated with water, so that the stress often reaches the rock failure threshold, which means that an earthquake occurs.

On the Geological and Mineral Map of Vietnam at the scale of 1:200,000 (Phong Sa Li - Dien Bien Phu sheet) [30], it can be seen that most of the reservoir area lies on the terrigenous sedimentary formations of the Da River formation ($P_{1\text{-}2}$ *sđ*) and the Nam Cuoi formation (S_2 - D_1 *nc*); the remaining small area lies on the formations of the Nam Po formation ($J_{1\text{-}2}$ *np*) and the Dien Bien complex ($\gamma\delta\nu P_3$-T_1 *đb*) (see Figure 4). The lithological composition of Da River formation consists of conglomerate, gritstone, quartzitic siltstone, shale, marl and limestone; the thickness of the formation is 1,200-2,300m. The Nam Cuoi formation is lithologically composed of shale, sericitized shale interspersed with sandstone, quartzitic sandstone, limestone; the thickness of the formation is 2,800-3,600m. The Nam Po formation is lithologically composed of coarse-grained sandstone interspersed with gritstone, silty sandstone, siltstone, and claystone. The Dien Bien complex is comprised of biotite granite, quartz diorite, granodiorite, gabbrodiorite, and diorite. According to the results of geological mapping at a scale of 1:50,000 (Muong Te sheet), the reservoir in the Muong Te commune area is located on the Nam Kha A formation ($C_{1\text{-}2}$ *nk*) which is mainly composed of sedimentary-eruptive materials such as basaltic tuff, rhyolitic tuff; the thickness of the formation is 400-520 m [31].

In addition, it can be seen from Figure 4 that along the reservoir from Muong Te town to Ka Lang commune, the granite intrusion of the Phu Si Lung complex (γaC_1 *pl*) is exposed about 5-7 km from the edge of the reservoir. This is a very large-scale magma intrusion. According to Thinh et al., (2005), at the cross section of Nam Kha A stream (Mu Ca commune), sedimentary rocks of the Da River and Nam Kha A

formations directly cover the granite of the Phu Si Lung complex; the granite massif of the Phu Si Lung complex causes hornification of sedimentary rocks of the Nam Cuoi formation [32]. Based on the order of the above-mentioned formations compared to the Phu Si Lung complex, it can be concluded that the granite massif of the Phu Si Lung complex is located below the upstream area of the reservoir at a depth of about 3,000-4,000 m. In Nam Khao and Muong Te communes have F-1, F-2, F-4 faults cross this granite massif, causing large fractures. When the water percolates down, these fractures will quickly become saturated with water. Accordingly, the stress in the massif will reach the failure threshold, which means the occurrence of an earthquake. In fact, after the Lai Chau reservoir filling, earthquakes have occurred along the reservoir from Kan Ho through Nam Khao to Muong Te and tend to develop gradually towards the Phu Si Lung granite intrusion massif (Figure 4).

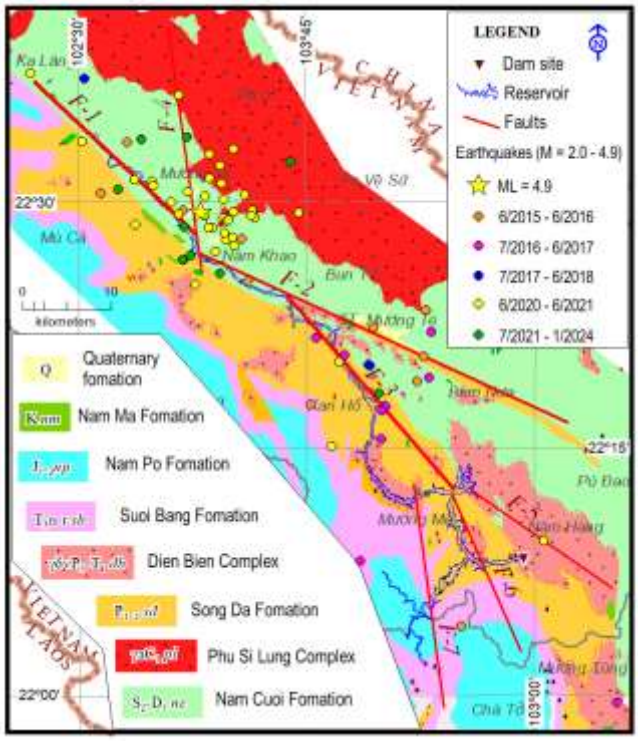

Figure 4. Location of Lai Chau reservoir on the Geological and Mineral Map of Vietnam at a scale of 1:200,000 (modified from Tuyet (Chief author), 2005).

3.2. Slip Tendency of Main Faults in the Reservoir Area

The SLIP TENDENCY program developed by Neves et al., (2009) [27] (a subroutine added to the COULOMB program by Toda et al., 2011 [33]) is used to analyze the slip tendency on the F-1, F-2, F-3, F-4, F-5, F-6 and F-7 faults in the Lai Chau reservoir area in 3D space. The input parameters used include: The orientation values of principal stress axes of regional tectonic stress field; The geometry of the main faults given in Table 1; and Young's modulus E = 800,000 bar; Poisson's ratio $\nu = 0.25$; Friction coefficient $\mu = 0.4$.

The regional tectonic stress field does not maintain a certain shape but changes over time, space and magnitude [34]. The best method to determine orientation values of three principal stress axes of modern regional tectonic stress field is based on the results of the analysis of

earthquake focal mechanisms [35-37]. When determining orientation values of three principal stress axes of tectonic stress field in the Vietnam - China - Laos border area, Wan et al., (2016) used the stress tensor inversion method on the dataset of focal mechanisms of 61 earthquakes [38]. The obtained results showed that the modern regional tectonic stress field has the maximum compressive principal stress axis (σ_1) oriented in the North Northwest - South Southeast and the maximum extensional principal stress axis (σ_3) oriented in the East Northeast - West Southwest. This result is also similar to the research results by [39, 40]; Hung (2002) when evaluating the state of three principal stress axes of tectonic stress field in the Northwest Vietnam [41]. Wan et al., (2016) determined the orientation values of three main stress axes of tectonic stress field in the Vietnam - China - Laos border area as follows: Maximum compressive principal stress axis σ_1 (ψ=349.5, δ=38); Maximum extensional principal stress axis σ_3 (ψ=80.4, δ=1.2); Intermediate principal stress axis σ_2 (ψ=172, δ=52) [38]. The study area in this paper is located entirely in the study area of [38]. Therefore, the orientation values of three principal stress axes of the modern regional tectonic stress field established by Wan et al. (2016) are used as input parameters in the analysis of slip tendency on faults in the Lai Chau reservoir area. The analysis results of the slip tendency of the main faults under the impact of modern regional tectonic stress field in the Lai Chau reservoir area are presented in Figure 5 below.

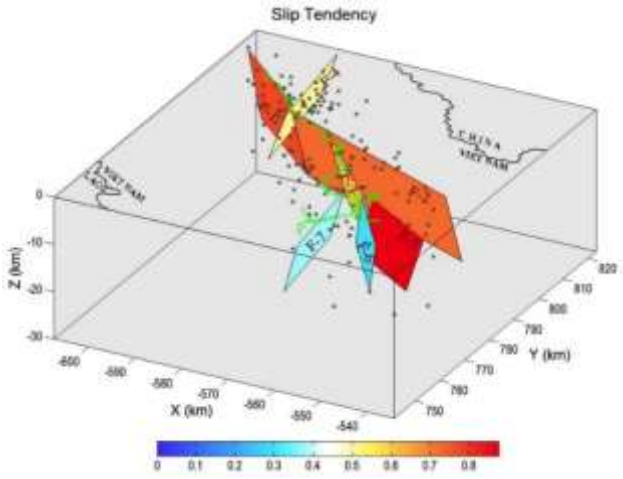

Figure 5. Slip tendency of main faults in Lai Chau reservoir area (red indicates faults with strong slip tendency).

Figure 5 indicates that the F-5 fault has an extremely strong slip tendency ($T_s \geq 0.8$), the F-1 and F-2 faults have a strong slip tendency (T_s = 0.7-0.8); the F-3 and F-4 faults have a medium slip tendency (T_s = 0.5-0.6); the F-6 and F-7 faults have a slight slip tendency (T_s = 0.3-0.4). Under the impact of modern regional tectonic stress field, the faults in the Lai Chau reservoir all tend to slip, which means the occurrence of earthquakes. This is clearly shown in Figure 5 earthquakes occur along the faults and are concentrated on the faults with strong slip tendency and large-scale such as the F-1 and F-2 faults. Although the F-5 fault exhibits the strongest slip tendency, earthquakes are rarely observed along it, possibly because it is a minor fault and lies mostly outside the reservoir area.

3.3. Coulomb Stress Change on Faults in the Reservoir Area

The COULOMB program developed by Toda et al., (2011) [33] is used to examine the

Coulomb stress change on faults in the Lai Chau reservoir at different depths. In addition to the input parameters given in Section 3.2, there is an important parameter which is the magnitude of the maximum earthquake occurring on the fault zone. The maximum earthquake scenario is assumed to occur on faults in the reservoir as follows: on F-1, F-2, F-3 faults, the magnitude of maximum earthquake is $M_{max} = 5.5 \pm 0.3$; and on F-4, F-5, F-6, F-7 faults, the magnitude of maximum earthquake is $M_{max} = 4.5 \pm 0.2$ [16, 19]. This scenario is inputted into the COULOMB program to calculate the stress change on the fault. The Coulomb stress change on the faults in the Lai Chau reservoir is calculated at depths of 10km and 15km and shown in Figure 6.

The results reveal that in the modern regional tectonic stress field, the Coulomb stress change appears at depths of 10km and 15km. The deeper it is, the greater the area of Coulomb stress change is. The Coulomb stress change is clearest and greatest at the intersection of three faults F-1, F-2, F-4. At this location, many earthquakes have occurred, including the event with magnitude M_L=4.9.

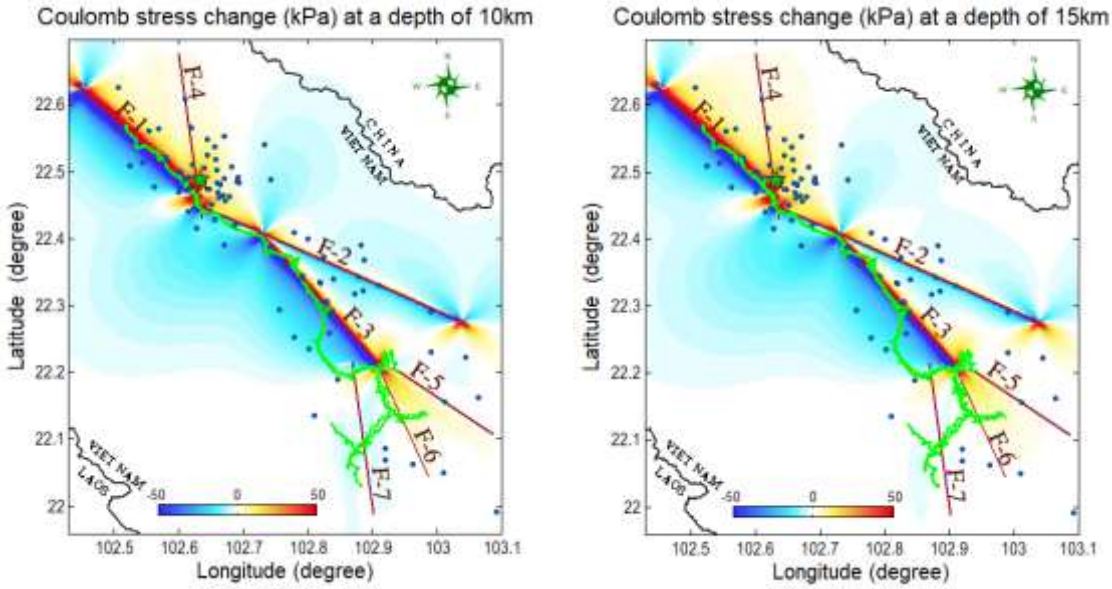

Figure 6. Coulomb stress change on main faults in the Lai Chau reservoir area (Red colour represents the increased stress; blue represents the decreased stress).

3.4. History of Reservoir Filling and Draining Cycle

Lai Chau reservoir is located in a region with the highland tropical characteristics - the Northwest Vietnam. The weather is divided into two distinct seasons: cold winter with low rainfall, hot - humid summer with heavy rainfall. Every year, the rainy season begins at the end of April and ends in October, coinciding with the prevailing southwest wind. The average annual rainfall ranges from 1,500 mm to over 3,000 mm. The average annual rainfall is about 2,531 mm, with the highest in July accounting for 87.5% of the annual rainfall. The dry season begins from November to March of the following year, with low rainfall (316.4 mm).

The data on average daily water level at Lai Chau reservoir provided by Lai Chau Operation Workshop of Son La Hydropower Company are used to construct a graph of the relationship between the reservoir filling and draining with the occurrence of earthquakes in the period from June 2015 to June 2024 (Figure 7).

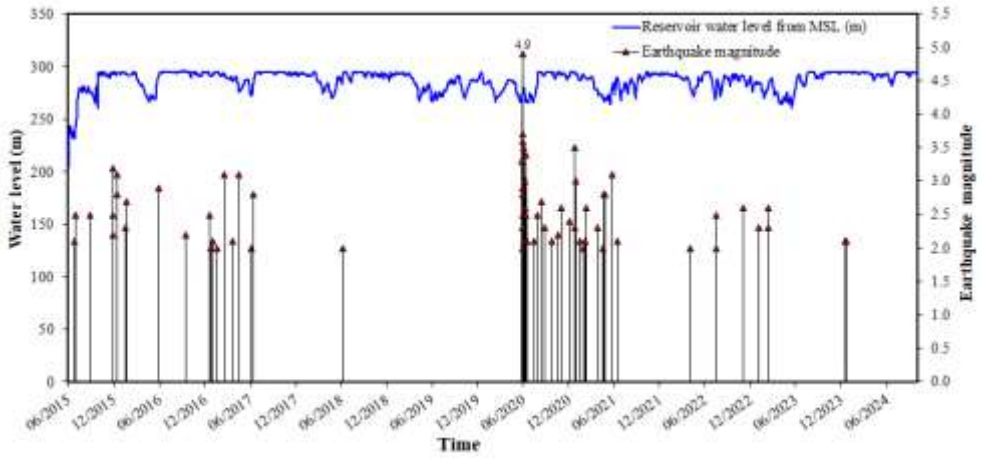

Figure 7. Relationship between water level fluctuations and earthquakes occurring in the Lai Chau reservoir area and its vicinity from June 2015 to June 2024.

Figure 7 reveals that the reservoir water level fluctuates very obviously according to the season. At the end of the dry season, the water level gradually decreases to an elevation of 265 m (MSL), and in the rainy season, the water level gradually increases in the second half of June every year. The water level usually peaks in late June and early July every year, and this water level maintains until the end of the dry season. Thus, June can be considered the beginning/end of a reservoir filling and draining cycle. From June 2015 to June 2019, the annual water level fluctuations of the reservoir occurred quite regularly. During this period, in the first two reservoir filling and draining cycles (June 2015 - June 2017), events with M_L = 2.0-3.2 appeared. In the next two cycles (6/2017 - 6/2019), only one event with M_L = 2.0 appeared. In the fifth cycle (6/2019 - 6/2020), the reservoir water level fluctuated continuously but no event with $M_L \geq 2.0$ occurred. In the sixth cycle (6/2020 - 6/2021), events with M_L = 2.0-4.9 appeared frequently. In the remaining three cycles (6/2021 - 6/2024), events with M_L = 2.0-3.1 occurred rarely and sporadically. Thus, it can be seen that fluctuations in the reservoir water level are related to earthquakes occurring during the reservoir filling and draining cycles, with the most evident correlation observed in the sixth cycle.

4. Discussion

The reservoir filling due to the hydropower dam construction certainly affects the state of accumulated stress on faults that were already near the failure threshold. Under the influence of the modern regional tectonic stress field, F-1, F-2, F-3, F-4 and F-5 faults all exhibit a moderate to strong tendency to slip (Figure 5). The strike-slip predominates in the slip mechanism of these faults. According to Roeloffs (1988), earthquakes are likely to occur below the reservoir if there is a vertical strike-slip fault [42]. With this characteristic, after the Lai Chau reservoir filled, the water percolated down along the fault surface, reducing the friction on the slip surface. Combined with water saturation in the fractures within Phu Si Lung granite intrusion, this process caused the accumulated stress to reach the failure threshold, creating favorable conditions for the slip on the faults to occur (i.e., earthquake occurrence). Moreover, the impact of the regional tectonic stress field also results in a considerable change in Coulomb stress on some faults in the upstream area of the reservoir (red-yellow area) (see Figure 6). Obviously, before reservoir filling, the Coulomb stress change was already present on the faults in this area. After reservoir filling, the Coulomb stress on the fault continues to change.

Thus, the reservoir filling has increased the accumulated stress on the faults to its failure threshold, triggered recent earthquakes in the reservoir area and its vicinity. This is evidenced by the focal mechanism of the event with M_L=4.9 that occurred on June 16, 2020 [43], which was determined to be right-lateral strike-slip with an additional reverse component (Table 3). This slip mechanism is consistent with that of the F-1 fault, indicating that the event M_L=4.9 likely occurred on the F-1 fault.

Table 3. Moment Tensor for Mw 4.7 (GCMT)
(according to http://ds.iris.edu/ds/products/momenttensor/18409916)

Event	Principal Axes				Nodal Planes				Focal Mechanism
	Name	Length	Plunge (°)	Azimuth (°)	Name	Strike (°)	Dip (°)	Rake (°)	
2020 06 16 06:12:29 GCMT: 22.42N 102.56E h=20.6 km Mw= 4.7 US: 22.462N 102.587E h=10 km mb= 4.5 IGP: 22.491N 102.634E h=10 km M_L = 4.9	T	1.562	25	234	NP1	15	60	7	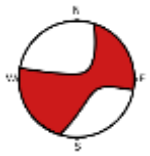
	N	0.216	60	92	NP2	282	84	150	
	P	-1.778	16	332					

The occurrence of earthquakes increased in number, frequency, and magnitude during the sixth reservoir filling and draining cycle, which was believed to be associated with reservoir operations during the fifth cycle. Figure 7 shows that the reservoir water level in the fifth cycle was unstable and fluctuated continuously (rising and falling). Moreover, the water level remained consistently low, which suddenly reduced the stress and pore water pressure that had already accumulated to high levels from previous cycles. This factor, combined with the aforementioned factors, triggered earthquakes in the second half of June and the subsequent months of the sixth reservoir filling and draining cycle. In this paper, we have not yet conducted an in-depth study on the change in pore water pressure. However, qualitatively, we believe that the event of M_L = 4.9 that occurred in the Lai Chau reservoir area (with a delay of 5 years since the first reservoir filling) is likely related to the diffusion of pore water pressure. This will be mentioned in the next study.

Due to the complexity and diversity of factors related to the occurrence of earthquakes, all assessments and studies to lessen the dangers caused by damming need to be considered simultaneously. This is enormously important because if any factor is considered separately or plays a leading role, it will be meaningless.

5. Conclusion

- At a depth of 3,000 - 4,000 meters beneath of the reservoir lies the granite massif of the Phu Si Lung complex, a type of rock that when water seeping down makes the stress in the rock easily reach the its failure threshold;
- Under the impact of the tectonic stress field in the Contemporary period, the F-1, F-2, F-3 and F-5 faults connected to the reservoir exhibit a strong slip tendency, accompanied by a clear Coulomb stress change on these faults.
- The intersection of the three faults F-1, F-2 and F-4 is where numerous earthquakes have occurred, including event of M_L = 4.9. At this location, the Coulomb stress change is also clearly observed and reaches its highest value.
- The unstable water level fluctuations in the fifth reservoir filling and draining cycle caused suddenly reduced the stress on the faults, thereby it triggered numerous earthquakes in the sixth cycle (in 2020).

- These factors interact with each other, contributing to favorable conditions for earthquakes to occur in the Lai Chau reservoir area and its vicinity. The numerous earthquakes that occurred during the period from June 2020 to June 2021 were related to reservoir water impoundment.

Acknowledgements

We would like to thank two anonymous reviewers for their helpful comments and the Son La Hydropower Company for providing data on daily water level of the Lai Chau hydropower reservoir to help us complete this article. This work was partially financed from PAS-VAST project no. QTPL01.01/22-23; Polish National Science Centre Grant no. 2021/41/B/ST10/02618; and the National-level Independent Project no. DTDLCN.58/22.

References

[1] P. Tapponnier, G. Peltzer, A. Ledain, P. Armijo, P. Cobbold, Propagating Extrusion Tectonics in Asia: New Insights from Simple Experiments with Plasticine, Geology, Vol. 10, No. 12, 1982, pp. 611-616.

[2] P. Tapponier, G. Peltzer, R. Armijo, On the Mechanics of the Collision Between India and Asia, Geological Society of London, Vol. 19, 1986, pp. 115-157.

[3] P. Tapponnier, R. Lacassin, P. H. Leloup, U. Schärer, D. Zhong, H. Wu, X. Liu, S. Ji, L. Zhang, J. Zhong, The Ailao Shan/Red River Metamorphic Belt: Tertiary Left-Lateral Shear Between Indochina and South China, Nature, Vol. 343, 1990, pp. 431-437.

[4] X. Qiu, Factors Controlling the Occurrence of Reservoir-Induced Seismicity, 1st Civil and Environmental Engineering Student Conference, 25-26 June 2012, Imperial College London, 2012, pp. 6.

[5] H. K. Gupta, A Review of Recent Studies of Triggered Earthquakes by Artificial Water Reservoirs with Special Emphasis on Earthquakes In Koyna, India, Earth-Science Reviews, Vol. 58, 2002, pp. 279-310.

[6] M. P. Wilson, G. R. Foulger, J. G. Gluyas, R. J. Davies, B. R. Julian, The Human-Induced Earthquake Database, Seismological Research Letters, Vol. 88, 2017, pp. 1560-1565.

[7] http://inducedearthquakes.org/, 2024 (accessed on: October 1st, 2024).

[8] N. N. Thuy, N. D. Xuyen, N. T. Tung, Triggered Earthquakes in Hoa Binh Reservoir. Vietnam Journal of Earth Sciences, Vol. 12, No. 4, 1993, pp. 93-97 (in Vietnamese).

[9] L. H. Minh, Results of Earthquake Survey in the Song Tranh 2 Hydropower Area in September 2012, http://www.vast.ac.vn/khoa-hoc-va-phat-trien/dieu-tra-co-ban/, 2012 (accessed on: October 1st, 2024) (in Vietnamese).

[10] C. D. Trieu, D. Q. Van, B. A. Nam, H. V. Long, The Initial Results of the Induce Earthquake Study in Song Tranh 2 Reservoir, Journal of Geology, Series A, Vol. 333, 2013, pp. 1-14 (in Vietnamese).

[11] B. V. Duan, H. T. Giang, N. A. Duong, P. D. Nguyen, About Factors Related to the Occurrence of Earthquakes in the Song Tranh 2 Hydropower Area in Period 2011-2014, Vietnam Journal of Earth Sciences, Vol. 37, No. 3, 2015, pp. 228-240, https://doi.org/10.15625/0866-7187/37/3/7797 (in Vietnamese).

[12] C. Lizurek, J. Wiszniowski, N. V. Giang, D. Q. Van, L. V. Dung, V. D. Tung, B. Plesiewicz, Background Seismicity and Seismic Monitoring in The Lai Chau Reservoir Area, J Seismol, Vol. 23, 2019, pp. 1373-1390, https://doi.org/10.1007/s10950-019-09875-6.

[13] L. Telesca, T. A. Tuan, C. D. Trong, C. D. Trieu, D. Q. Van, M. X. Bach, Fractal and Spectral Analysis of Seismicity in the Lai Chau Area (Vietnam), Fractal Fract, Vol. 7, 2023, pp. 15, https://doi.org/10.3390/fractalfract7110776.

[14] N. N. Thuy, Detailed Zoning for Earthquake Forecasting in The Northwest Region, Final Report of State-Level Science and Technology Project, coded KC08-10, Archived at Institute of Geophysics, VAST, Hanoi, 2005, pp. 526 (in Vietnamese).

[15] T. V. Thang, P. D. Linh, L. T. Viet, V. D. Tung, N. T. T. Huong, Results of Geological and Tectonic Surveys and Assessment of Regional Tectonic Activity, Establishment of Tectonic Fault Maps at a Scale of 1: 50,000 for the Region and a Scale of 1: 10,000 for the Profile. Serving the Preparation of the Report on Determining Design Earthquake Parameters (Supplementary), in Lai Chau Hydropower Plant Project, Technical Design Stage, Archived at the Institute of Geophysics,

Vietnam Academy of Science and Technology, Hanoi, 2009, pp. 43 (in Vietnamese).

[16] L. T. Son, Report on Determining Design Earthquake Parameters (Supplementary), in Lai Chau Hydropower Plant Project, in Technical Design Stage, Archived at the Institute of Geophysics, Vietnam Academy of Science and Technology, Hanoi, 2009, pp. 89 (in Vietnamese).

[17] N. X. Thanh et al., Synthesis and Assessment of Active Fault Systems in the Area and Compilation of the Seismogenic Fault Map for Muong Te District and Surrounding Areas, Scale 1: 25,000, Scientific report under the Special and Potential Research Project; Code: 01/2021/DX, Funded by the National Foundation for Science and Technology Development (NAFOSTED), Ministry of Science and Technology, Archived at the Institute of Geophysics, Vietnam Academy of Science and Technology, Hanoi, 2021, pp. 99 (in Vietnamese).

[18] N. D. Xuyen, N. N. Thuy, Database for Solutions to Mitigate the Consequences of Earthquakes in Vietnam, Final Report of the State-Level Independent Project, Coded KT-DL 92-07, Institute of Geophysics, Vietnam Academy of Science and Technology, Hanoi, 1996, pp. 117 (in Vietnamese).

[19] N. D. Xuyen, Earthquake and Ground Motion Forecasting in Vietnam, Final Report of State-Level Independent Project, Archived at Institute of Geophysics, Vietnam Academy of Science and Technology, Hanoi, 2004, pp. 209 (in Vietnamese).

[20] http://www.isc.ac.uk/iscbulletin/search/catalogue/, 2024 (accessed on: October 1st, 2024).

[21] P. T. Truyen, Assessment of the Causes of the Earthquake in Muong Te on June 16, 2020, and Proposal of Risk Mitigation Measures. Synthesis report of the Special and Potential Research Project; Code: 01/2021/DX, Funded by the National Foundation for Science and Technology Development (NAFOSTED), Ministry of Science and Technology, Archived at the Institute of Geophysics, Hanoi, Vietnam Academy of Science and Technology, Hanoi, 2023, pp. 252 (in Vietnamese).

[22] S. Toda, J. Lin, M. Meghraoui, R. S. Stein, 12 May 2008 M = 7.9 Wenchuan, China, Earthquake Calculated to Incr Ease Failure Stress and Seismicity Rate on Three Major Fault Systems, Geophysical Research Letters, Vol. 35, 2008, pp. 1-6, https://doi.org/10.1029/2008GL034903.

[23] Y. Okada, Internal Deformation Due to Shear and Tensile Faults in A Half-Space, Bulletin of the Seismological Society of America, Vol. 82, No. 2, 1992, pp. 1018-1040, https://doi.org/10.1785/BSSA0820021018.

[24] G. C. P. King, R. S. Stein, J. Lin, Static Stress Changes and the Triggering of Earthquakes: Bulletin of the Seismological Society of America, Vol. 84, No. 3, 1994, pp. 935-953, https://doi.org/10.1785/BSSA0840030935 .

[25] T. Parsons, C. Ji, E. Kirby, Stress Changes from the 2008 Wenchuan Earthquake and Increased Hazard in The Sichuan Basin, Nature, Vol. 454, No. 7203, 2008, pp. 509-510, https://doi.org/10.1038/nature07177.

[26] A. Morris, D. Ferril, D. Henderson D., Slip-Tendency Analysis and Fault Reactivation, Geology, Vol. 24, 1996, pp. 275-278.

[27] M. Neves, L. Paiva, J. Luis, Software for Slip-Tendency Analysis in 3D: A Plug-In for Coulomb. Computers and Geosciences, Vol. 35, 2009, pp. 2345-2352.

[28] W. S. Fyfe, N. J. Price, A. B. Thompson, Fluids in Earth's Crust: Their Significance in Metamorphic, Tectonic and Chemical Transport Processes, Elsevier Scientific Publishing Company, 1978, pp. 383.

[29] F. Cornet, J. Yin, 1995. Analysis of Induced Seismicity for Stress Field Determination and Pore Pressure Mapping, Pure Appl. Geophys, Vol. 145, No. 3, 1995, pp. 677-700.

[30] T. D. Tuyet, Vietnam Seismic and Mineral Map, at a Scale of 1:200,000, Phong Sa Ly - Dien Bien Phu Sheet, Department of Geology and Minerals of Vietnam. Hanoi, 2005 (in Vietnamese).

[31] L. Hung, Geological and Mineral Map, Muong Te Sheets, at Scale 1/50,000, Archived at The Department of Geology, Hanoi, 2001 (in Vietnamese).

[32] D. D. Thinh, L. Hung, V. X. Dinh, C. V. Lam, D. T. Y. Ngoc, N. Phuong, D. D. Nguyen, N. T. Toan, New Data on Geology and Minerals in Muong Te Area, Lai Chau - Dien Bien, Journal of Geology, Vol. 289, 2005, pp. 22-28 (in Vietnamese).

[33] S. Toda, R. S. Stein, V. Sevilgen, J. Lin, Coulomb 3.3 Graphic-rich Deformation and Stress-Change Software-User Guide: U.S. Geological Survey Open-File Report 2011-1060, 2011, pp. 63, Available at: http://pubs.usgs.gov/of/2011/1060/ (accessed on: October 1st, 2024).

[34] B. Andeweg, G. Vicente, S. Cloetingh, J. Giner, A. M. Martin, Local Stress Field and Intraplate Deformation of Iberia: Variations in Spatial and Temporal Interplay of Regional Stress Sources, Tectonophysics, Vol. 305, 1999, pp. 153-164.

[35] H. Moghimi, M. Arian, A. Sorbi, Fault Movement Potential of Marzanabad Area, North Alborz, Iran, Open Journal of Geology, Vol. 5, 2015, pp. 126-135, https://doi.org/10.4236/ojg.2015.53012.

[36] P. T. Trinh, An Inverse Problem for the Determination of the Stress Tensor from Polyphased Fault Sets and Earthquake Focal Mechanisms, Elsevier Science Publishers B.V., Amsterdam, Tectonophysics, Vol. 224, 1993, pp. 393-411.

[37] A. Sorbi, M. Arian, M. Pourkermani, The Movement Potential Evaluation of the Major Quaternary Faults in Tehran Quadrangle, Journal of Sciences - Islamic Azad University (JSIAU), Vol 19, No. 73, 2009, pp. 176-182.

[38] Y. G. Wan, S. Z. Sheng, J. C. Huang, X. Li, X. Chen, The Grid Search Algorithm of Tectonic Stress Tensor Based on Focal Mechanism Data and Its Application in the Boundary Zone of China, Vietnam and Laos, Journal of Earth Science, Vol. 27. No. 5, 2016, pp. 777-785, https://doi.org/10.1007/s12583-015-0649-1.

N. T. Yem, Tectonic Stress Field Regimes in Cenozoic in Vietnam Territory, Journal of Geology, Series A, Vol. 236, 1996, pp. 1-6 (in Vietnamese).

[39] R. H. Findlay, P. T. Trinh, The Structural Setting of Song Ma Region, Vietnam and the Indochina-South China Plate Boundary Problem, Gondwana Research, Vol. 1, No. 1, 1997, pp.11-33.

[40] N. V. Hung, Basic Characteristics of the Northwest Neotectonic Faults, PhD Thesis in Geology, Institute of Geology, Vietnam Academy of Science and Technology, Hanoi, 2002 (in Vietnamese).

[41] E. A. Roeloffs, Fault Stability Changes Induced Beneath A Reservoir With Cyclic Changes in Water Level, Journal Geophys. Res., Vol. 93, 1988, pp. 2107-2124, https://doi.org/10.1029/JB093iB03p02107.

[42] http://ds.iris.edu/ds/products/momenttensor/#citation/, 2024 (accessed on: October 1st, 2024).

Appendix:

Catalog of earthquakes with M ≥ 2.0 in Lai Chau reservoir area and its vicinity from 1900 to June 2024

No.	Year	Month	Date	Hr.	Min.	Sec.	Long.	Lat.	Depth (km)	Mag.	Type of M
1	1961	11	26	15	7	0	22.5	102.6	15	4.1	Ms
2	1977	7	15	14	16	53	22.33	102.91	5	3.4	Ms
3	1978	10	7	12	25	0	22.39	102.67	5	3.2	Ms
4	1980	6	17	22	16	0	22.29	102.99	10	4.2	Ms
5	1981	12	18	13	10	22	22.23	102.99	5	3.2	Ms
6	1985	8	19	13	41	19	22.4	102.8	10	4.7	Ms
7	1996	11	13	18	51	46	22.34	102.84	5.9	4.6	Ms
8	2001	1	5	18	20	43	22.05	103.01	10	2.8	Ms
9	2001	11	28	3	29	15	22.47	102.6	2	3.9	Ms
10	2005	9	26	13	48	13	22.409	102.778	13	3.6	Ms
11	2006	1	6	18	28	10	22.235	102.801	7.7	4	Ms
12	2006	1	23	21	9	20	22.086	102.919	17.1	2.9	Ms
13	2007	6	7	5	31	14	22.163	103.065	17	3.3	Ms
14	2009	3	27	14	43	37	22.189	102.845	10	3.6	Ms
15	2014	10	19	17	34	2	22.222	103.044	10	3.5	M_L
16	2014	11	26	14	21	24.8	22.062	102.962	5.7	2	M_L
17	2015	7	15	3	33	50.6	22.463	102.679	15.1	2.1	M_L
18	2015	7	20	12	36	41.8	22.069	102.92	10	2.5	M_L
19	2015	9	14	20	4	15.7	22.492	102.615	19.3	2.5	M_L
20	2015	12	14	8	4	49.8	22.561	102.553	8.2	3.2	M_L
21	2015	12	15	22	51	30.8	22.343	102.879	10	2.5	M_L
22	2015	12	16	3	52	45.9	22.318	102.872	14.7	2.2	M_L
23	2016	1	2	8	46	18.9	22.509	102.524	14.3	3.1	M_L

No.	Year	Month	Date	Hr.	Min.	Sec.	Long.	Lat.	Depth (km)	Mag.	Type of M
24	2016	1	2	8	46	25.2	22.294	102.755	10	2.8	M_L
25	2016	2	4	9	41	42	22.39	102.882	3.1	2.3	M_L
26	2016	2	9	0	19	55.9	22.373	102.824	10	2.7	M_L
27	2016	6	17	3	5	54.1	22.42	102.686	10.1	2.9	M_L
28	2016	10	3	19	46	49.7	22.335	102.818	15	2.2	M_L
29	2017	1	7	22	23	48	22.322	102.885	10	2.5	M_L
30	2017	1	13	4	36	49	22.135	102.809	10	2	M_L
31	2017	1	18	11	36	9	22.292	102.837	14	2.1	M_L
32	2017	2	6	19	0	0	22.288	102.833	11	2	M_L
33	2017	3	6	3	37	1	22.362	102.761	15	3.1	M_L
34	2017	4	8	16	2	9	22.368	102.887	13.6	2.1	M_L
35	2017	5	5	7	50	42	21.991	103.092	10	3.1	M_L
36	2017	5	19	20	36	32	22.259	102.832	10.5	2.9	M_L
37	2017	6	24	3	3	22	22.345	102.792	8.1	2	M_L
38	2017	7	1	11	25	0	22.626	102.506	12	2.8	M_L
39	2018	6	25	12	1	4.2	22.334	102.82	10	2	M_L
40	2020	6	15	16	43	16.6	22.464	102.669	11.9	3.3	M_L
41	2020	6	16	6	12	29	22.491	102.634	10	4.9	M_L
42	2020	6	16	6	13	3	22.456	102.671	8	3.7	M_L
43	2020	6	16	8	54	59.9	22.469	102.66	12	2	M_L
44	2020	6	16	11	23	28.3	22.474	102.647	12.8	2.3	M_L
45	2020	6	16	15	3	28.7	22.519	102.657	7.6	2.5	M_L
46	2020	6	16	18	9	30.8	22.474	102.643	12.5	2	M_L
47	2020	6	16	20	47	43.1	22.537	102.655	6	2.8	M_L
48	2020	6	18	19	16	41.4	22.492	102.691	6.2	2.3	M_L
49	2020	6	18	22	1	21.5	22.503	102.659	10	2.9	M_L
50	2020	6	19	1	9	26.1	22.416	102.628	13.8	3.6	M_L
51	2020	6	22	15	20	35.5	22.45	102.65	14.3	3.5	M_L
52	2020	6	24	6	59	44.9	22.486	102.639	3.7	2.1	M_L
53	2020	6	27	12	37	35.2	22.252	102.778	9	2.1	M_L
54	2020	6	28	4	41	14	22.5	102.602	5.5	2.6	M_L
55	2020	6	28	23	48	38.7	22.609	102.61	14.8	3	M_L
56	2020	7	1	23	7	24.9	22.631	102.447	7	2.5	M_L
57	2020	7	2	15	16	35.4	22.462	102.662	2.4	3.4	M_L
58	2020	7	3	22	53	27.4	22.484	102.659	9.7	2.1	M_L
59	2020	8	3	19	26	18.2	22.481	102.663	10.6	2.1	M_L
60	2020	8	16	13	58	16.5	22.549	102.644	2.5	2.5	M_L
61	2020	8	31	9	27	58.6	22.554	102.67	2.8	2.7	M_L
62	2020	9	13	4	44	52.4	22.484	102.693	12.4	2.3	M_L
63	2020	10	13	5	33	14.8	22.338	102.786	7.6	2.1	M_L
64	2020	11	6	7	1	8.7	22.508	102.682	15	2.2	M_L
65	2020	11	18	0	45	31.2	22.562	102.504	7.3	2.6	M_L
66	2020	12	23	7	5	22.1	22.156	103.011	3.6	2.4	M_L
67	2021	1	11	5	32	9.6	22.517	102.582	14.2	2.3	M_L
68	2021	1	12	21	17	27.3	22.511	102.62	8.1	3.5	M_L

No.	Year	Month	Date	Hr.	Min.	Sec.	Long.	Lat.	Depth (km)	Mag.	Type of M
69	2021	1	15	15	8	28	22.49	102.67	10.5	3	M_L
70	2021	2	4	20	35	27.7	22.521	102.58	14.3	2.1	M_L
71	2021	2	17	5	6	15.5	22.506	102.639	7.7	2	M_L
72	2021	2	22	15	1	7.9	22.482	102.664	9.5	2.1	M_L
73	2021	2	27	18	34	47.3	22.524	102.644	16.1	2.6	M_L
74	2021	4	15	13	20	40.6	22.523	102.561	8	2.3	M_L
75	2021	5	6	20	13	57.1	22.488	102.61	8	2	M_L
76	2021	5	10	23	25	9.3	22.486	102.69	13.9	2.8	M_L
77	2021	5	15	8	4	31.5	22.489	102.742	10	2.8	M_L
78	2021	6	14	22	5	51	22.477	102.562	9.3	3.1	M_L
79	2021	7	5	23	7	3.8	22.475	102.616	10	2.1	M_L
80	2022	4	20	21	55	19.1	22.564	102.569	1.4	2	M_L
81	2022	8	5	16	47	11.9	22.428	102.655	10	2	M_L
82	2022	8	6	15	39	53	22.306	102.83	2.4	2.5	M_L
83	2022	11	20	19	31	24.9	22.541	102.733	10	2.6	M_L
84	2023	1	21	19	22	16.2	22.446	102.623	1.7	2.3	M_L
85	2023	3	2	21	57	22.4	22.441	102.615	5	2.6	M_L
86	2023	3	2	22	48	30.2	22.441	102.614	6	2.3	M_L
87	2024	1	4	13	36	17.3	22.566	102.619	1.6	2.1	M_L